National Synchrotron Radiation Research Center

Soft X-ray Absorption and Resonant Scattering

Di-Jing Huang *djhuang@nsrrc.org.tw*

Nat'l Synchrotron Radiation Research Center, Taiwan
Dept. of Physics, Nat'l Tsing Hua University, Taiwan

Cheiron 2009, SPring-8, Japan
Oct. 3

1

Soft X-ray Absorption and Resonant Scattering

1. Soft X-ray Absorption
   - Basic
   - Experimental Setup
   - Applications
     - Chemical analysis
     - Orbital polarization
     - Magnetic Circular Dichroism
2. Resonant Soft X-ray Scattering
   - Introduction
   - Basic of resonant X-ray scattering
   - Examples:
   - Magnetic Transition of a Quantum Multiferroic $LiCu_2O_2$

2

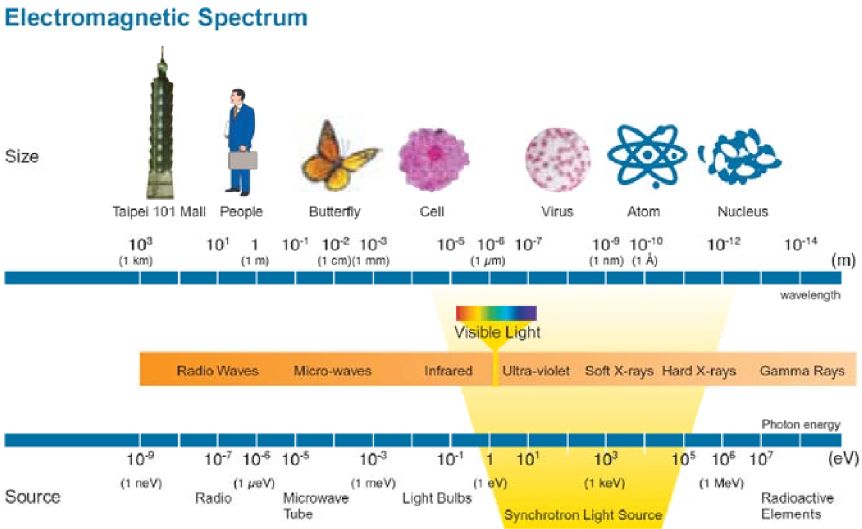

Soft x-ray: 250 eV ~ a few keV

3

Interaction of photons with matter:

Photoelectric effect

Photoabsorption

Scattering/diffraction

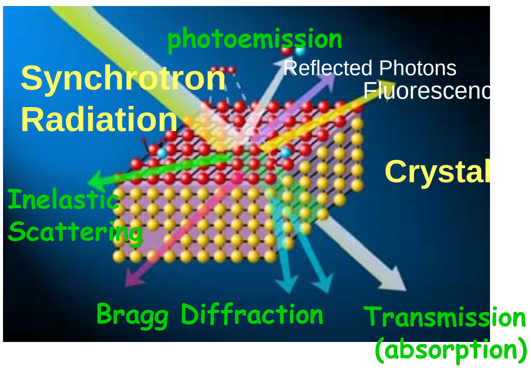

- **lattice structure: arrangement of atoms**
- **electronic states**
- **magnetic order**
- **excitations (electronic states or phonons)**

4

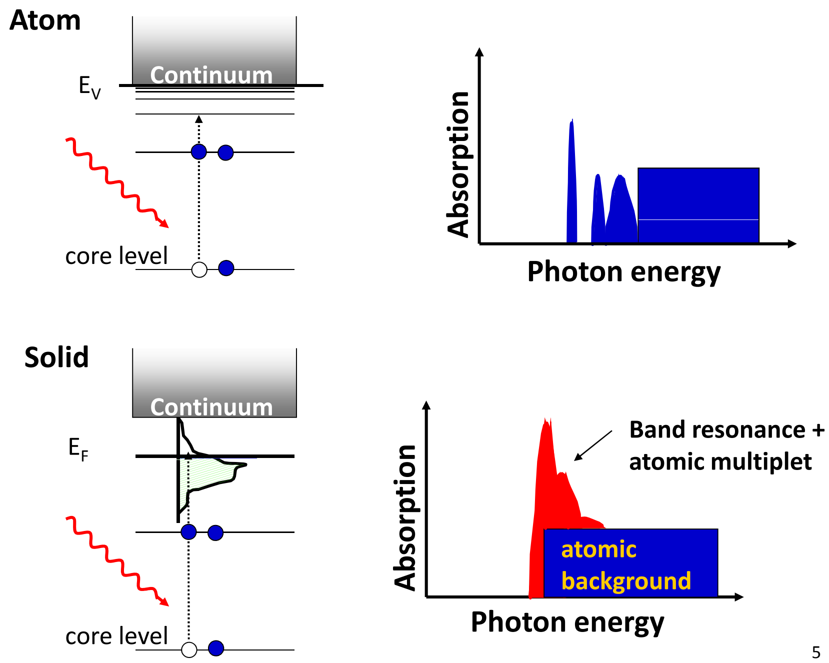

5

Photo-absorption $\quad \dfrac{d\sigma}{d\Omega} \propto \sum \left| \langle \Psi_f | \mathbf{A} \cdot \mathbf{P} | \Psi_i \rangle \right|^2 \cdot \delta\left(E_f - E_i - h\nu\right)$

If $\mathbf{k} \cdot \mathbf{r} << 1$, **Dipole approximation:** $\quad e^{i\mathbf{k}\cdot\mathbf{r}} \approx 1 + i\mathbf{k}\cdot\mathbf{r} \approx 1$

$$\mathbf{A} = \boldsymbol{\varepsilon} e^{i(\mathbf{k}\cdot\mathbf{r} - \omega t)} \approx \boldsymbol{\varepsilon} e^{-i\omega t}$$

polarization of x-ray

$$\frac{d\sigma}{d\Omega} \propto \sum \left| \langle f | \boldsymbol{\varepsilon} \cdot \mathbf{P} | i \rangle \right|^2 \cdot \delta\left(E_f - E_i - h\nu\right)$$

$$\propto \sum \left| \langle f | \boldsymbol{\varepsilon} \cdot \mathbf{r} | i \rangle \right|^2 \cdot \delta\left(E_f - E_i - h\nu\right)$$

$$\because \langle f | \boldsymbol{\varepsilon} \cdot \mathbf{P} | i \rangle \approx \frac{im}{\hbar} \boldsymbol{\varepsilon} \cdot \langle f | [\hat{H}, \mathbf{r}] | i \rangle$$

$$= \frac{im}{\hbar}(E_f - E_i) \boldsymbol{\varepsilon} \cdot \langle f | \mathbf{r} | i \rangle = im\omega \langle f | \boldsymbol{\varepsilon} \cdot \mathbf{r} | i \rangle$$

$$[\hat{H}, \mathbf{r}] = \frac{\hbar}{i} \frac{\mathbf{P}}{m}, \quad \text{if } [V(r), \mathbf{r}] = 0$$

<u>**Absorption probability:**</u>

$$W = \frac{2\pi}{\hbar} \left| M_{ij} \right|^2 \delta(\hbar\omega - E_f + E_i) \qquad M_{ij} \propto \langle f | \boldsymbol{\varepsilon} \cdot \hat{\mathbf{r}} | i \rangle$$

6

Dipole transition

Absorption probability: $W = \frac{2\pi}{\hbar}\left|M_{ij}\right|^2 \delta(\hbar\omega - E_f + E_i)$ $\quad M_{ij} \propto \langle f | \boldsymbol{\varepsilon}\cdot\hat{\mathbf{r}} | i \rangle$

$$\boldsymbol{\varepsilon}\cdot\hat{\mathbf{r}} = e_x \sin\boldsymbol{\theta}\cos\boldsymbol{\phi} + e_y \sin\boldsymbol{\theta}\sin\boldsymbol{\phi} + e_z \cos\boldsymbol{\theta}$$

$$\hat{\mathrm{r}} = (\sin\theta\cos\phi, \sin\theta\sin\phi, \cos\theta)$$

$$\cos\theta = \sqrt{\tfrac{4\pi}{3}}Y_{1,0}(\theta,\phi) \qquad \sin\theta\cdot e^{\pm i\phi} = \mp\sqrt{\tfrac{8\pi}{3}}Y_{1,\pm1}(\theta,\phi)$$

$$\boldsymbol{\varepsilon}\cdot\hat{\mathrm{r}} = \sqrt{\tfrac{4\pi}{3}}\left(\frac{-\varepsilon_x + i\varepsilon_y}{\sqrt{2}}Y_{1,1} + \frac{\varepsilon_x + i\varepsilon_y}{\sqrt{2}}Y_{1,-1} + \varepsilon_z Y_{1,0}\right)$$

$$\langle \psi_{l',m'} | \mathbf{Y}_{1,\pm1} | \psi_{l,m} \rangle \neq 0$$

when

Dipole allowed transition 2p → 3d:

$$\Delta m \equiv m' - m = \pm 1$$

$$\Delta l \equiv l' - l = 1$$

$$M_{ij} \propto \langle 2p^5 3d^{n+1} | \boldsymbol{\varepsilon}\cdot\mathbf{r} | 2p^6 3d^n \rangle$$

L. circularly polarized:
$\Delta m_l = +1$ ($\because$ $Y_{1,1}$)

R. circularly polarized:
$\Delta m_l = -1$ ($\because$ $Y_{1,-1}$)

7

Dipole allowed transitions :

$1s \rightarrow np$ **K-edge XAS can be accurately described with single-particle methods.**

$2p \rightarrow 3d$ **L-edge XAS: the single-particle approximation breaks down and the pre-edge structure is affected by the core hole wave function. The multiplet effect exists.**

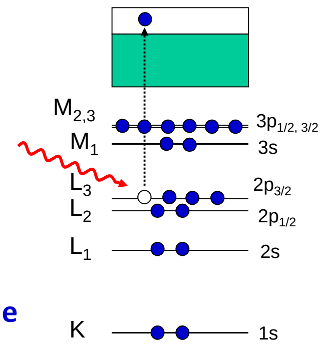

8

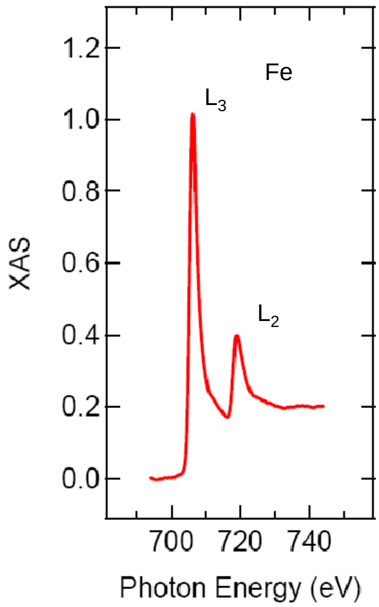

- Two absorption "peaks" from $2p \rightarrow 3d$:

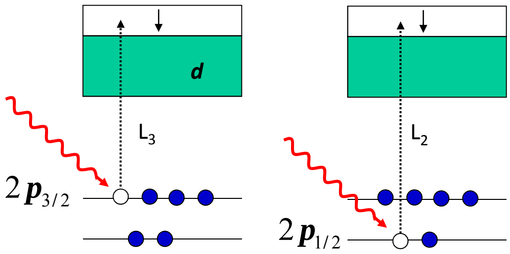

- **Absorption cross section is proportional to numbers of d holes and density of states in the core level.**
- **L-edge XAS provides information on the chemical state, orbital symmetry, and spin state of materials.**

9

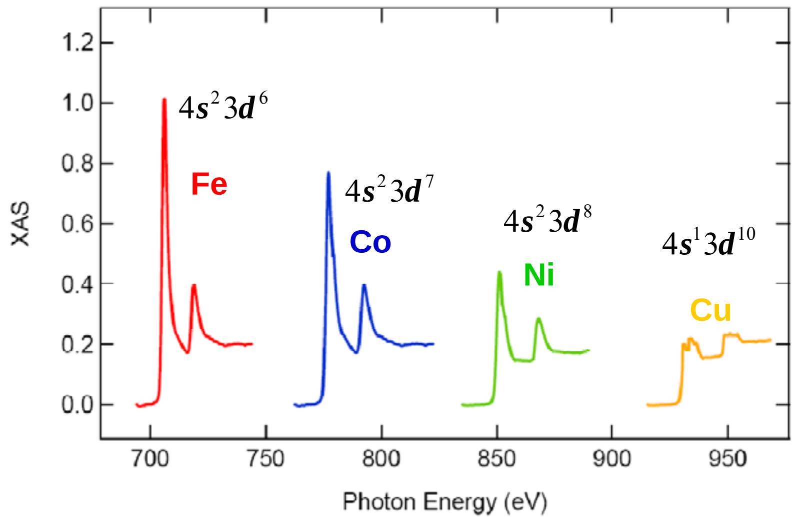

Each element has specific absorption energies.
"finger print" → element specific spectroscopy

10

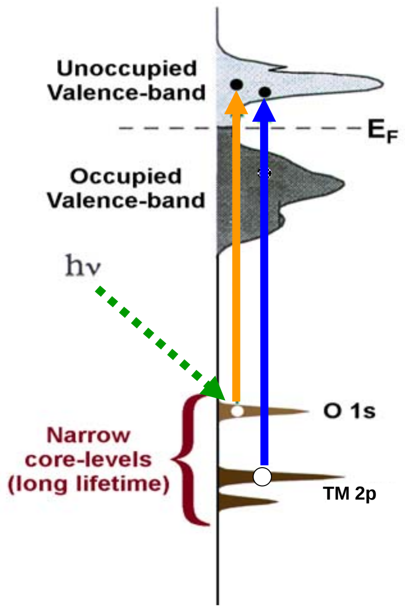

In transition-metal oxides

- **soft x-ray absorption & scattering:**
  TM: 2p → 3d
  O: 1s → 2p
- **direct, element-specific probing of electronic structure of TMO**

11

Soft X-ray Absorption and Resonant Scattering

1. Soft X-ray Absorption
   - Basic
   - **Experimental Setup**
   - Applications
     - Chemical analysis
     - Orbital polarization
     - Magnetic Circular Dichroism
2. Resonant Soft X-ray Scattering
   - Introduction
   - Basic of resonant X-ray scattering
   - Examples:
   - Magnetic Transition of a Quantum Multiferroic $LiCu_2O_2$

12

Measurement of Soft X-ray Absorption

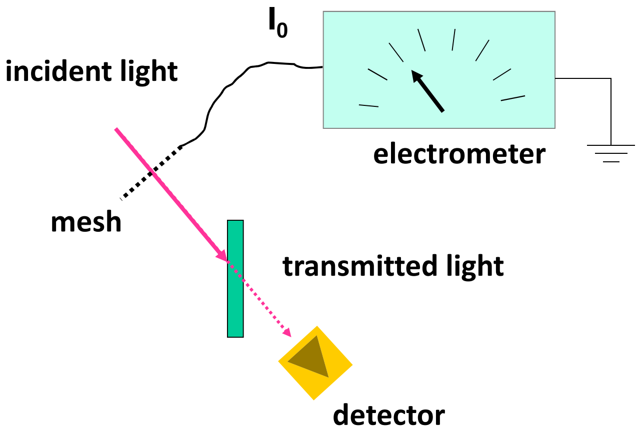

13

Photoexcitation and Relaxation

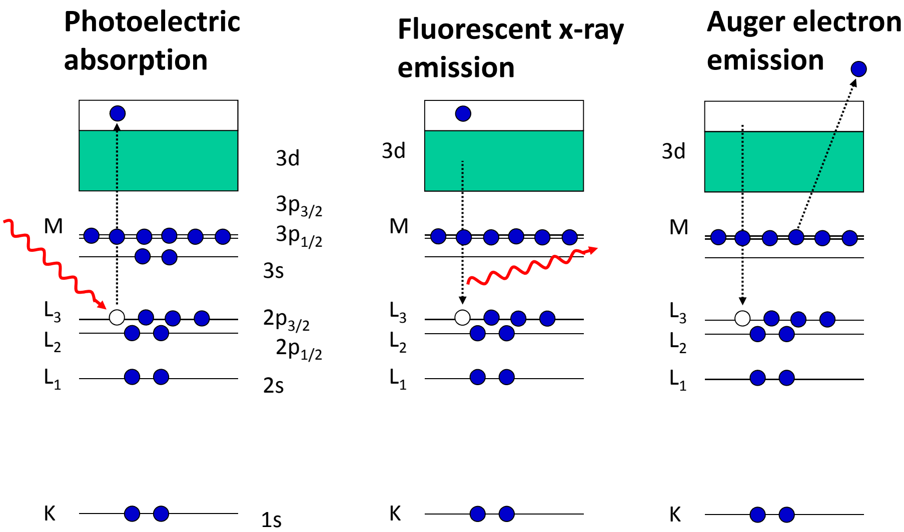

14

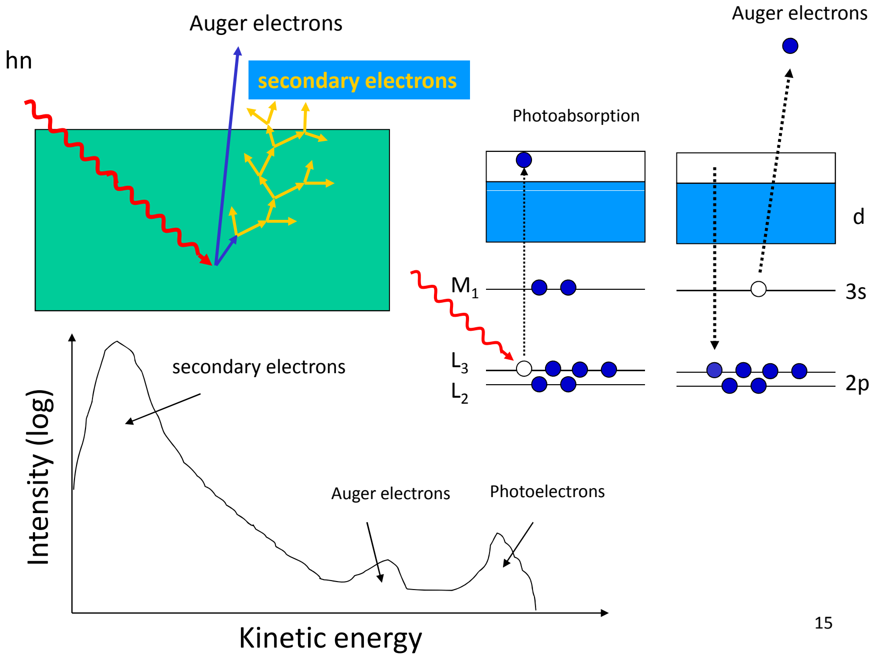

15

Measurement of Soft X-ray Absorption

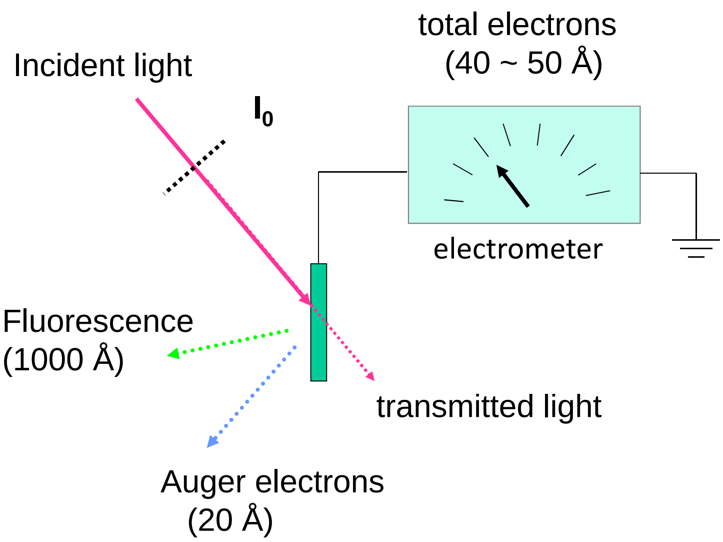

16

L-edge XAS provides information on the chemical state, orbital symmetry, and spin state of materials.

17

Soft X-ray Absorption and Resonant Scattering

1. Soft X-ray Absorption
   - Basic
   - Experimental Setup
   - Applications
     - Chemical analysis
     - Orbital polarization
     - **Magnetic Circular Dichroism**
2. Resonant Soft X-ray Scattering
   - Introduction
   - Basic of resonant X-ray scattering
   - Examples:
   - Magnetic Transition of a Quantum Multiferroic $LiCu_2O_2$

18

Polarization of Synchrotron Radiation

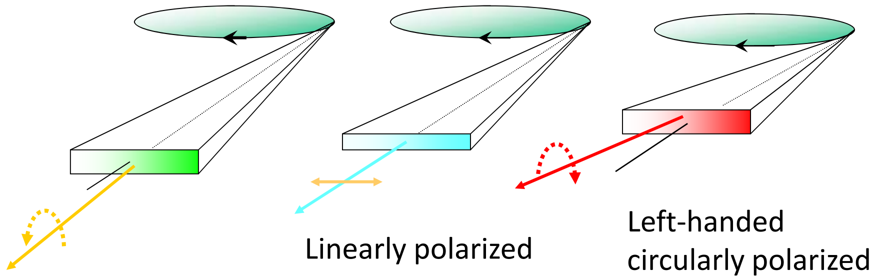

Soft X-Ray Magnetic Circular Dichroism in Absorption

For $2p_{3/2} \rightarrow 3d$

Right-handed circularly polarized light preferentially excites spin-down electrons.

Left-handed circularly polarized light preferentially excites spin-up electrons.

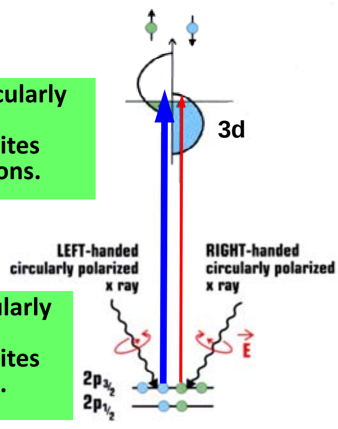

$L_3 \rightarrow 3d$

For spin up,

$$\frac{\text{left-handed}}{\text{right-handed}} = 5/3$$

For spin down

$$\frac{\text{left-handed}}{\text{right-handed}} = 3/5$$

Soft X-Ray Magnetic Circular Dichroism in Absorption

For $2p_{3/2} \rightarrow 3d$

Right-handed circularly polarized light preferentially excites spin-down electrons.

Left-handed circularly polarized light preferentially excites spin-up electrons.

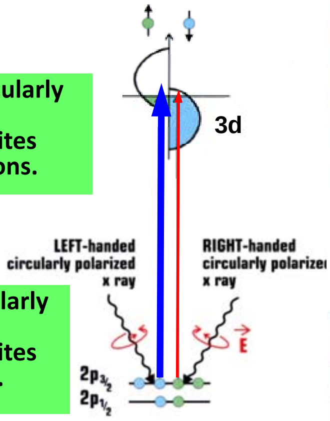

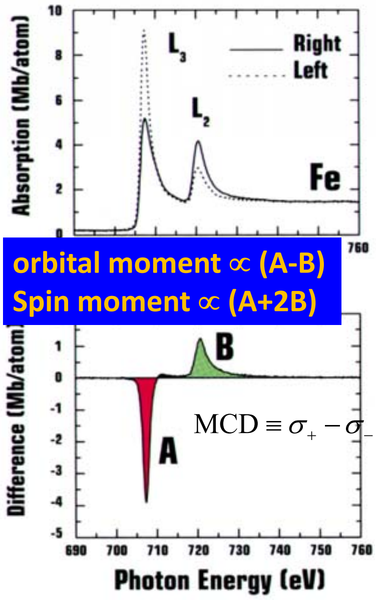

MCD is defined as the difference in absorption intensity of magnetic systems excited by left- and right-handed circularly polarized light.

Soft X-Ray Magnetic Circular Dichroism in Absorption

Soft X-ray MCD in absorption provides a unique means to probe:

- element-specific magnetic hysteresis
- orbital and spin moments
- magnetic coupling.

There are two ways to obtain a MCD spectrum:

1) Fixing M, measure XAS with left and right circular lights.
2) Fixing the helicity of light, measure XAS with two opposite directions of M.

Element-Specific Magnetic Hysteresis Measurements

A New Technique for Studying Interlayer Magnetic Coupling

Chen et al., PRB 48, 642 (1993)

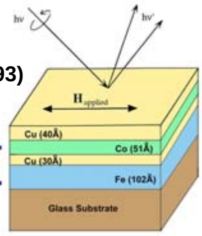

SXMCD Hysteresis Curves

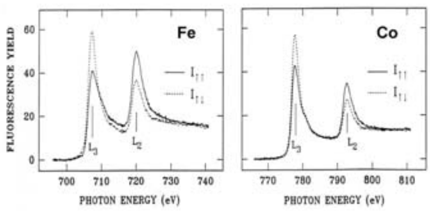

Conventional Hysteresis C

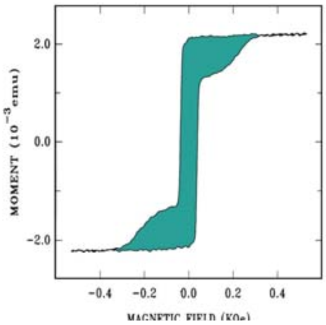

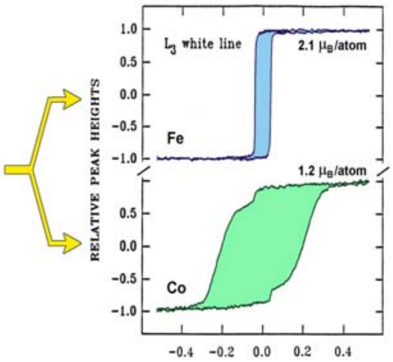

Ferromagnetism in one-dimensional monatomic metal chains

P. Gambardella*, A. Dallmeyer†, K. Maiti†, M. C. Malagoli†, W. Eberhardt†‡, K. Kern*§ & C. Carbone†||

Nature 416, 301 (2001)

Two-dimensional systems, such as ultrathin epitaxial films and superlattices, display magnetic properties distinct from bulk materials[1]. A challenging aim of current research in magnetism is to explore structures of still lower dimensionality[2–6]. As the dimensionality of a physical system is reduced, magnetic ordering tends to decrease as fluctuations become relatively more important[7]. Spin lattice models predict that an infinite one-dimensional linear chain with short-range magnetic interactions spontaneously breaks up into segments with different orientation of the magnetization, thereby prohibiting long-range ferromagnetic order at a finite temperature[7–9]. These models, however, do not take into account kinetic barriers to reaching equilibrium or interactions with the substrates that support the one-dimensional nanostructures. Here we demonstrate the existence of both short- and long-range ferromagnetic order for one-dimensional monatomic chains of Co constructed on a Pt substrate. We find evidence that the monatomic chains consist of thermally fluctuating segments of ferromagnetically coupled atoms which, below a threshold temperature, evolve into a ferromagnetic long-range-ordered state owing to the presence of anisotropy barriers. The Co chains are characterized by large localized orbital moments and correspondingly large magnetic anisotropy energies compared to two-dimensional films and bulk Co.

a

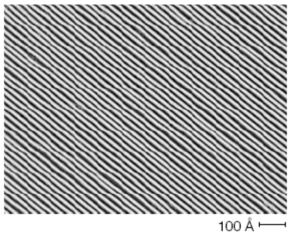

b

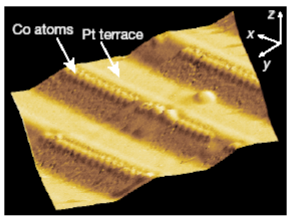

Figure 1 STM topographs of the Pt(997) surface. **a**, Periodic step structure (each white line represents a single step). The surface has a 6.45° miscut angle relative to the (111) direction; repulsive step interactions result in a narrow terrace width distribution centred at 20.2 Å with 2.9 Å standard deviation. **b**, Co monatomic chains decorating the Pt step edges (the vertical dimension is enhanced for better contrast). The monatomic chains are obtained by evaporating 0.13 monolayers of Co onto the substrate held at $T = 260$ K and previously cleaned by ion sputtering and annealing cycles in ultrahigh vacuum (UHV). The chains are linearly aligned and have a spacing equal to the terrace width.

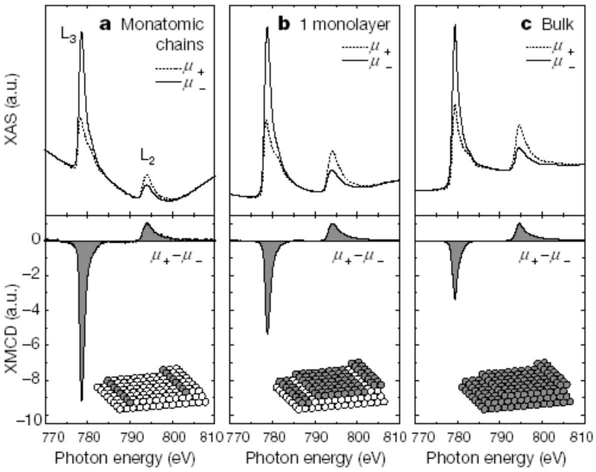

Figure 2 Co X-ray absorption spectra for parallel (μ_+) and antiparallel (μ_-) direction of light polarization and field-induced magnetization. The dichroism signal ($\mu_+ - \mu_-$) is obtained by subtraction of the absorption spectra in each panel and normalization to the L_2 peak. **a**, Monatomic chains; **b**, one monolayer; **c**, thick Co film on Pt(997). The sample was mounted onto a UHV variable-temperature insert that could be rotated with the respect to the direction of the external magnetic field applied parallel to the incident photon beam. Spectra were recorded in the electron-yield mode at $T = 10$ K and

25

Soft X-ray Absorption and Resonant Scattering

1. Soft X-ray Absorption
   - Basic
   - Experimental Setup
   - Applications
     - Chemical analysis
     - Orbital polarization
     - Magnetic Circular Dichroism
2. Resonant Soft X-ray Scattering
   - Introduction
   - Basic of resonant X-ray scattering
   - Examples:
   - Magnetic Transition of a Quantum Multiferroic $LiCu_2O_2$

26

Spin, Charge, and orbital ordering of correlated electron systems

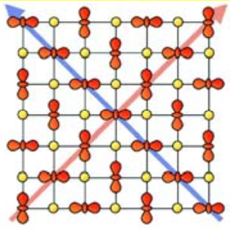

$La_{0.5}Sr_{1.5}MnO_4$

Murakami et al. (1998)

Moritomo et al. (1995) Sternlieb et al. (1996)

$La_{1/3}Ca_{2/3}MnO_3$

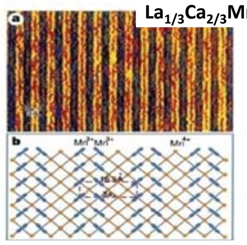

C. H. Chen et al. (1998)

$La_{1.6-x}Nd_{0.4}Sr_xCuO_4$

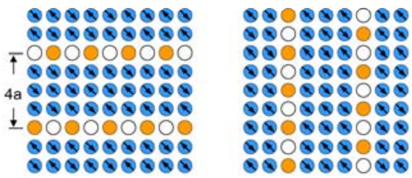

J. Tranquda et al. (1995)

modulation vector $k = 2\pi/\lambda$

Small valence disproportionation !

$\Delta Q/Q_{total} \ll 1$

Elastic x-ray scattering

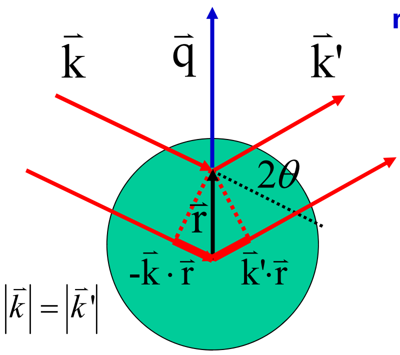

momentum transfer

$$\hbar\vec{q} = \hbar\vec{k}' - \hbar\vec{k}$$

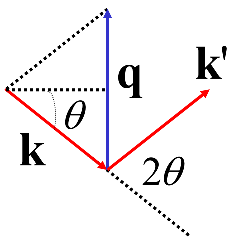

$$q = 2k\sin\theta = \frac{4\pi}{\lambda}\sin\theta$$

A volume element $d^3\vec{r}$ at $\vec{r}$ will contribute an amount to the scattering field with a phase factor $e^{i\vec{q}\cdot\vec{r}}$.

scattering form factor

$$f_q \equiv \sum_j \rho(\vec{r}_j) e^{i\vec{q}\cdot\vec{r}_j}$$

$$\frac{d\sigma}{d\Omega} \propto |f_q|^2$$

Fourier transform of charge distribution.

Resonant scattering

As the photon energy $\hbar\omega$ approaches the binding energy of one of the core-level electrons,

$$f_s(\mathbf{q},\hbar\omega) = f^0(\mathbf{q}) + \underbrace{f'(\hbar\omega) + i\,f''(\hbar\omega)}_{\text{dispersion corrections}}$$

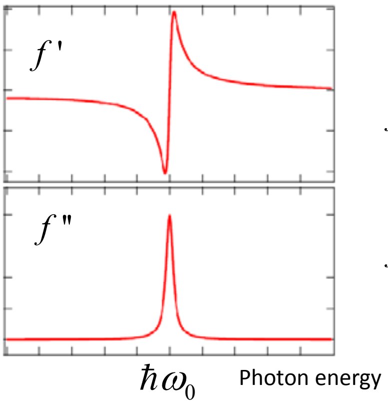

$$f' = \frac{\omega_s^2(\omega^2-\omega_s^2)}{(\omega^2-\omega_s^2)^2+(\omega\Gamma)^2}$$

$$f'' = -\frac{\omega_s^2\omega\Gamma}{(\omega^2-\omega_s^2)^2+(\omega\Gamma)^2}$$

Absorption

$$\sigma = -\frac{4\pi}{k}\mathrm{Im}(f)$$

29

Advantage of Resonant Soft X-ray Scattering

$$\boldsymbol{f}_{res} \sim \sum_{3d} \frac{\left\langle \Psi_{2p} \middle| \vec{\varepsilon}\cdot\vec{\boldsymbol{r}}\boldsymbol{e}^{i\vec{k}'\cdot\vec{r}} \middle| \Psi_{3d} \right\rangle \left\langle \Psi_{3d} \middle| \vec{\varepsilon}_0\cdot\vec{\boldsymbol{r}}\boldsymbol{e}^{i\vec{k}\cdot\vec{r}} \middle| \Psi_{2p} \right\rangle}{\hbar\omega - (\boldsymbol{E}_{3d} - \boldsymbol{E}_{2p} - \boldsymbol{i}\Gamma)}$$

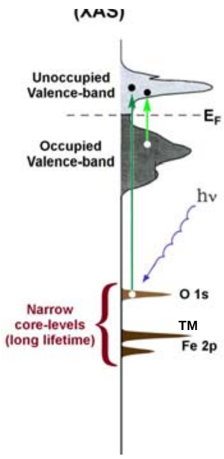

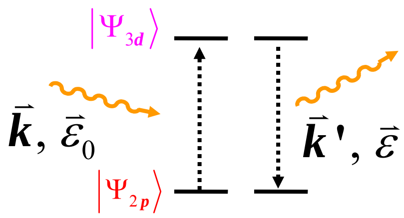

momentum transfer

$$\vec{q} \equiv \vec{k}' - \vec{k}$$

→ modulation vector

- **With $\hbar\omega = E_{3d} - E_{2p}$, f_{res} is enhanced dramatically and ordering of Ψ_{3d} is focused.**

30

Resonant X-ray magnetic scattering

electric dipole transitions

Hannon et al., PRL(1988)

$$f_{mag}^{res} = -i\frac{3\lambda}{8\pi}(\varepsilon^{*} \times \varepsilon_0)\cdot \hat{z}(F_{1,1} - F_{1,-1})$$

$\Delta m_l = 1$ $\quad$ $\Delta m_l = -1$

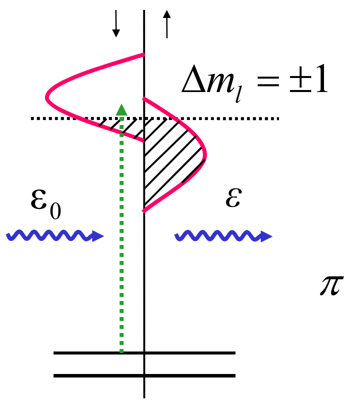

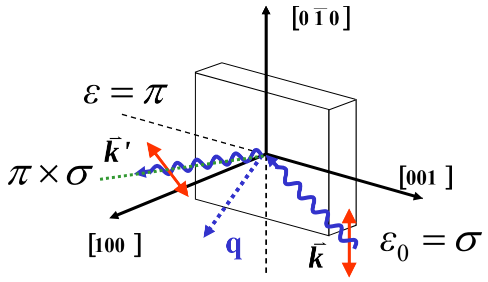

As a result of spin-orbit and exchange interactions, magnetic ordering manifests itself in resonant scattering.

31

<u>Resonant soft x-ray magnetic scattering:</u>

•Cross section comparable to that of neutron scattering.

•Good q resolution (Δq < 0.0005 Å^{-1})

•Spectroscopic information.

•Limited to a small k space, less bulk sensitive.

32

Setup of Soft X-ray Scattering

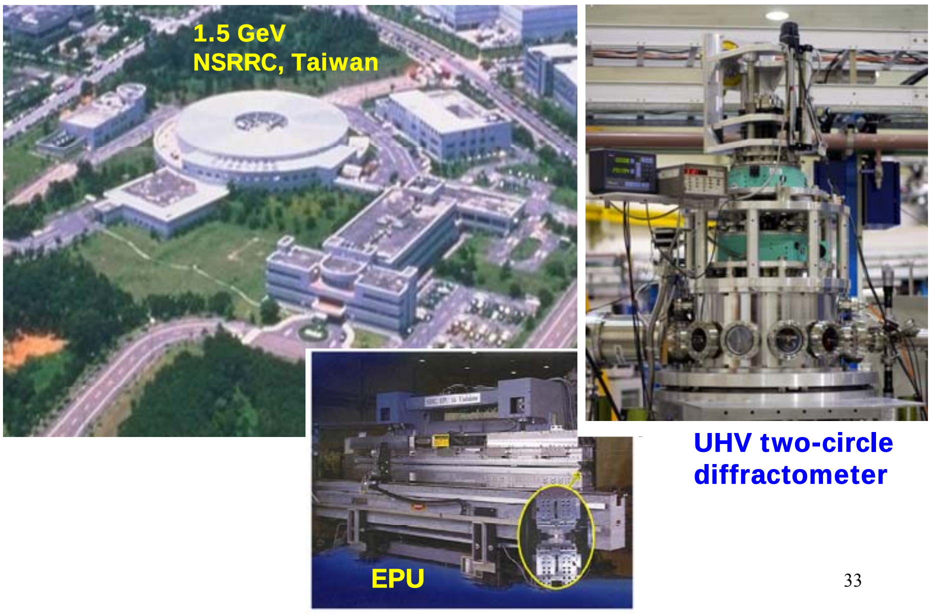

UHV two-circle diffractometer

33

Soft X-ray Absorption and Resonant Scattering

1. Soft X-ray Absorption
   - Basic
   - Experimental Setup
   - Applications
     - Chemical analysis
     - Orbital polarization
     - Magnetic Circular Dichroism
2. Resonant Soft X-ray Scattering
   - Introduction
   - Basic of resonant X-ray scattering
   - **Examples:**
   - **Magnetic Transition of a Quantum Multiferroic $LiCu_2O_2$**

34

Magnetism: ordering of spins

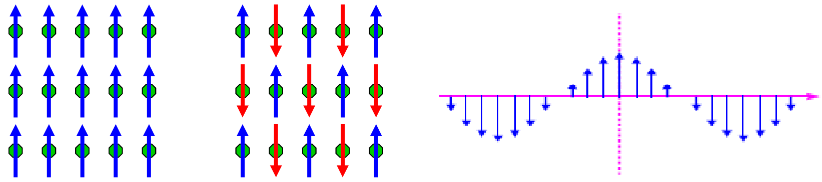

Magnetization can be induced by H field

Ferroelectricity: polar arrangement of charges

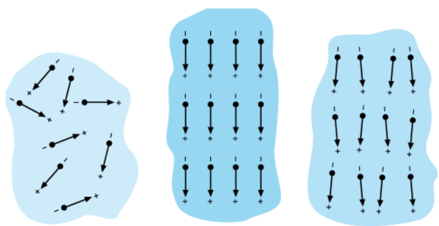

Electric polarization can be induced by E field

35

Magnetoelectric effect

Induction of magnetization by an electric field; induction of polarization by a magnetic field.

- first presumed to exist by Pierre Curie in 1894 on the basis of symmetry considerations

Multiferroics: materials exhibiting ME coupling

Cr_2O_3
$BiMnO_3$
$BiFeO_3$
…..

However, the effects are typically too small to be useful in applications!

36

Two contrasting order parameters

Magnetization: time-reversal symmetry broken

$$t \Rightarrow -t: \quad \vec{M} \Rightarrow -\vec{M}$$

$$\vec{P} \Rightarrow \vec{P}$$

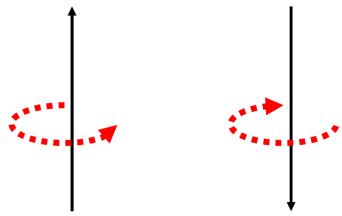

Polarization: inversion symmetry broken

$$\vec{r} \Rightarrow -\vec{r}: \ \vec{P} \Rightarrow -\vec{P}, \ \vec{M} \Rightarrow \vec{M}$$

$$\vec{P} = q\vec{r}$$

37

Recently discovery in the coexistence and gigantic coupling of antiferromagnetism and ferroelectricity in frustrated spin systems such $RMnO_3$ and RMn_2O_5 (R=Tb, Ho , …)

$TbMnO_3$: Kimura et al., Nature 426, 55, (2003)
$TbMn_2O_5$: Hur et al., Nature 429, 392 (2004)

revived interest in "multiferroicity"

Magnetism and ferroelectricity coexist in materials called "multiferroics."

- **$T_C < T_N$**
- **Ferroelectricity is induced magnetism.**

38

Electric polarization reversal and memory in a multiferroic material induced by magnetic fields

N. Hur, S. Park, P. A. Sharma, J. S. Ahn*, S. Guha & S-W. Cheong

$TbMn_2O_5$ Nature, 429, 392 (2004)

- 3 transitions on cooling.
- Magnetic field induces a sign reversal of the electric polarization.

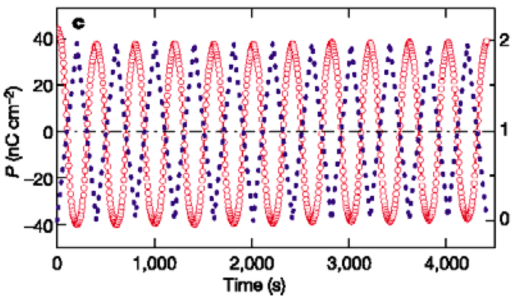

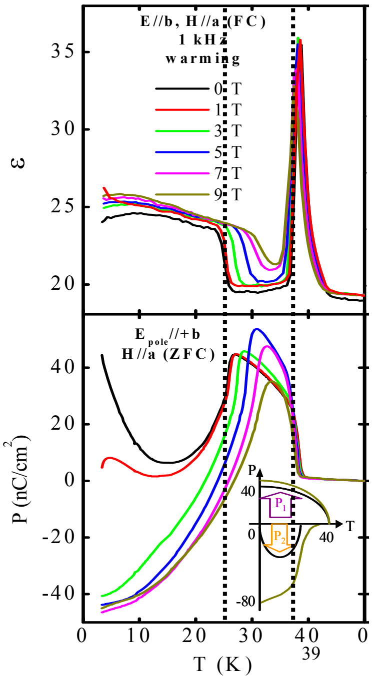

39

Quantum multiferroic magnet $LiCu_2O_2$

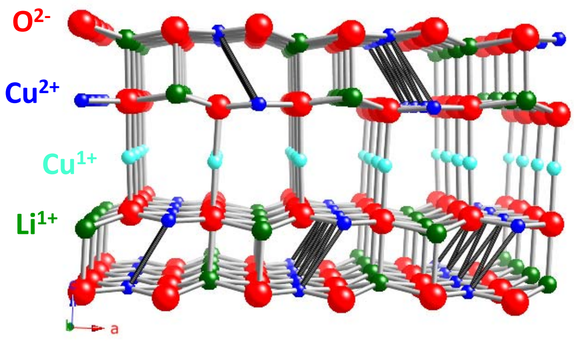

orthorhombic, *Pnma*
a=5.734 Å,
b=2.856 Å,
c=12.415 Å

Qausi-1D spin ½ chain:
- **Characterization of the ground state?**
- **Multiferroicity**

(Park et al. PRL98, 057601; Seki et al., PRL (2008); cond-mat 0810.2533

40

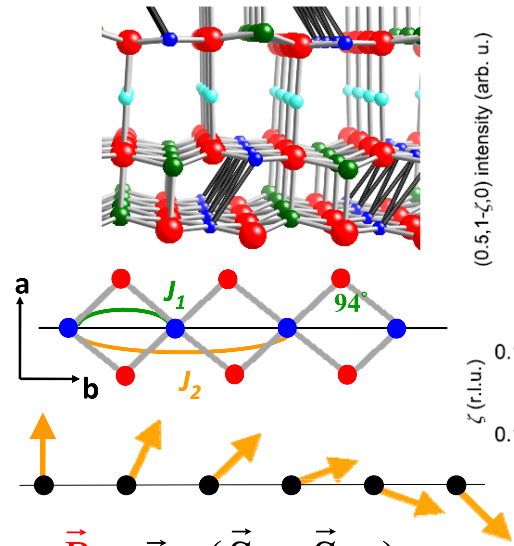

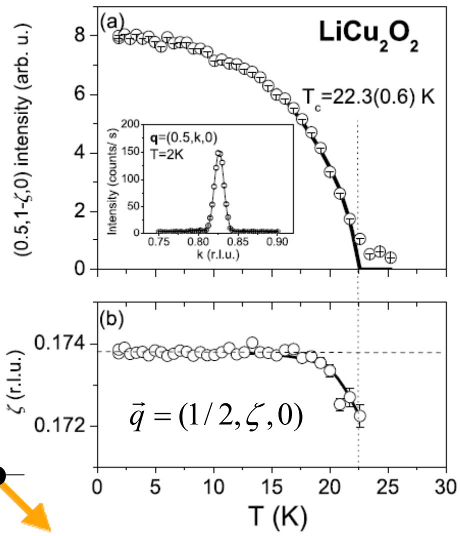

$$\vec{P} \propto \vec{e} \times (\vec{S}_n \times \vec{S}_{n+1})$$

$\vec{q} = (1/2, \zeta, 0)$

in units of $(\frac{2\pi}{a}, \frac{2\pi}{b}, \frac{2\pi}{c})$

along the a axis ?

Masuda et al., PRL (2004)

41

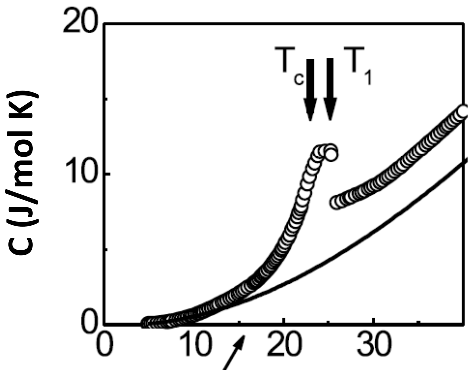

Two transitions ?

Masuda et al., PRL (2004)

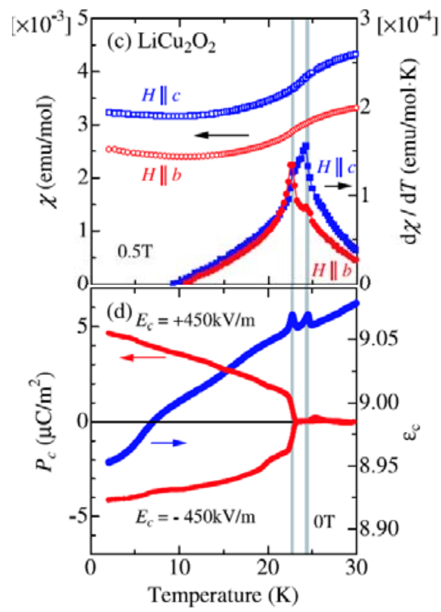

Seki et al., PRL (2008)

42

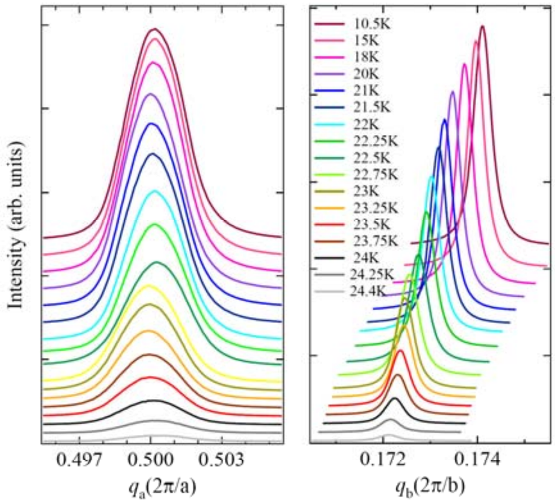

$LiCu_2O_2$ (100) single crystal

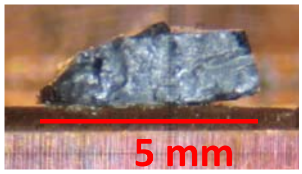

Resonant soft x-ray magnetic scattering

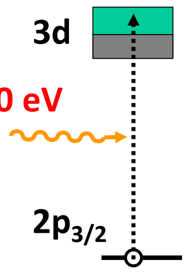

Correlation length ξ = 1/HWHM

T = 10K: ξ_a = 690 Å ξ_b = 2100 Å

43

q_a (2p/a)

$\vec{q} = (1/2, \zeta, 0)$

q_b (2p/b)

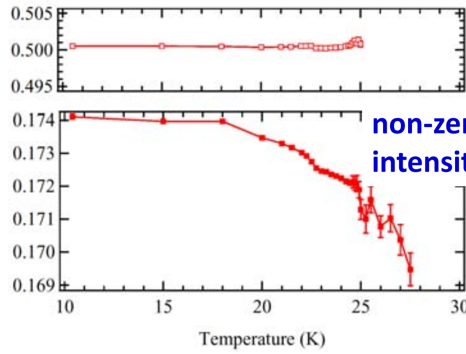

non-zero scattering intensity above T_N

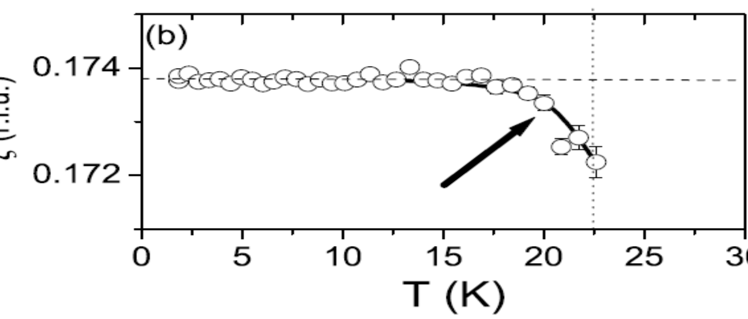

Masuda et al., PRL (2004)

44

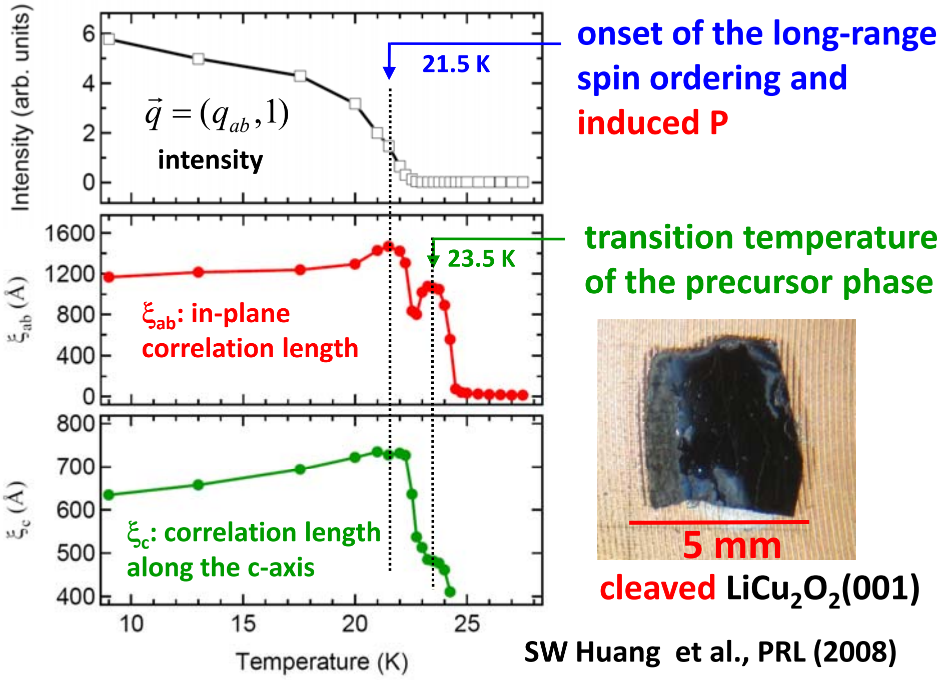
onset of the long-range spin ordering and induced P
21.5 K
$\vec{q} = (q_{ab}, 1)$
intensity
Intensity (arb. units)
transition temperature of the precursor phase
23.5 K
ξ_{ab}: in-plane correlation length
ξ_{ab} (Å)
ξ_c: correlation length along the c-axis
ξ_c (Å)
Temperature (K)
5 mm
cleaved $LiCu_2O_2$(001)
SW Huang et al., PRL (2008)

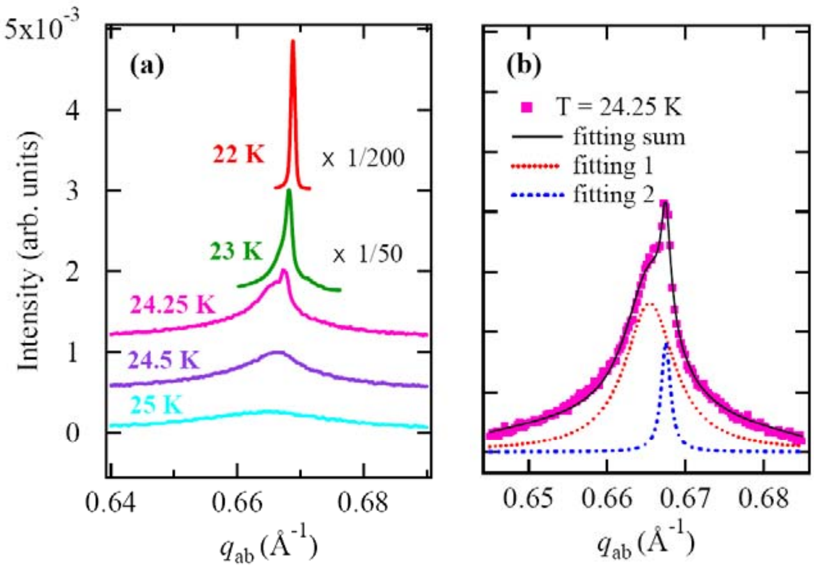
(a)
5×10^{-3}
Intensity (arb. units)
22 K
x 1/200
23 K
x 1/50
24.25 K
24.5 K
25 K
q_{ab} (Å^{-1})
(b)
T = 24.25 K
fitting sum
fitting 1
fitting 2
q_{ab} (Å^{-1})

46

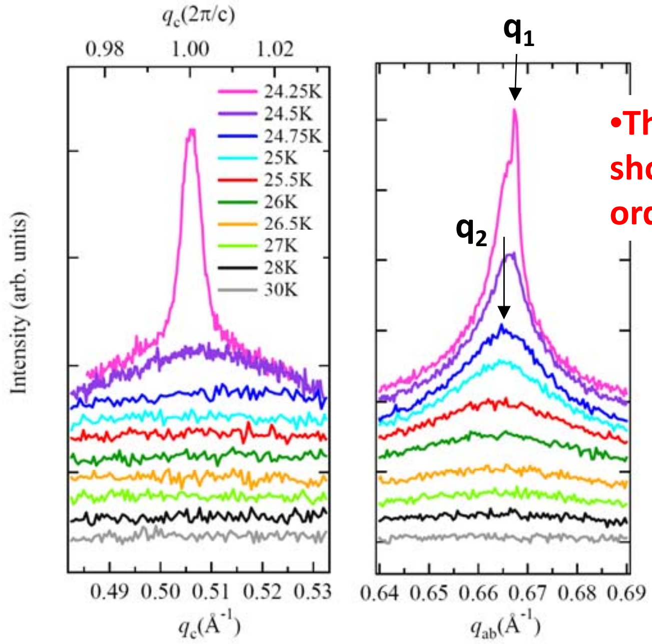

$$\vec{q} = (q_{a,b}, 1)$$

- There is an in-plane short-range AFM ordering above T_N
- extension of the zero-temperature AFM ordering
- spin coupling along the c axis is essential for inducing P.

47

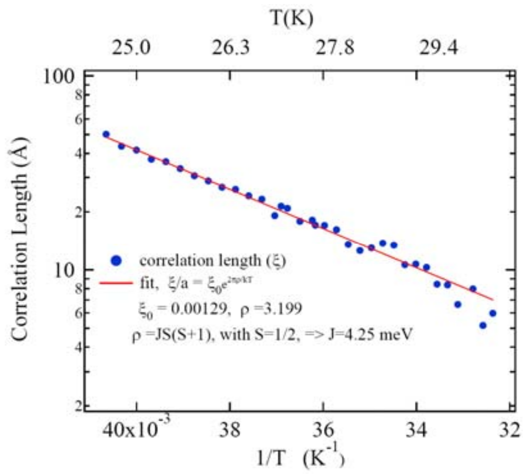

Above T_N, in-plane correlation

$$\xi(T) \propto e^{2\pi\rho_S / k_B T}$$

2D renormalized classical behavior

average
J ~ 4.25 meV

- The ground state of $LiCu_2O_2$ exhibits a long range AFM ordering.
- The spin coupling along the c axis is essential for inducing P.

48

Thank you!

49

Appendix: Basic of Magnetic Circular Dichroism in X-ray Absorption

Considering L-edge $2p_{3/2} \rightarrow 3d$ absorption, and ignoring the spin-orbit interaction in the 3d bands,

$$\sigma \propto \left| \langle l, m_l \,|\, \boldsymbol{\varepsilon} \cdot \hat{\mathbf{r}} \,|\, j, m_j \rangle \right|^2$$

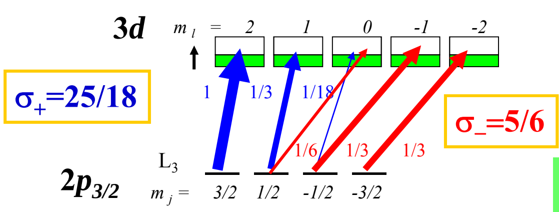

For left-handed circular light

$$\sigma_+ \propto R(r)^2 \cdot \left| \langle Y_{lm} \,|\, \frac{\varepsilon_x - i\varepsilon_y}{\sqrt{2}} Y_{1,1} \,|\, j, m_j \rangle \right|^2$$

radial part

Left-handed circularly polarized light preferentially excites spin-up electrons.

For light-handed circular light

$$\sigma_- \propto R(r)^2 \cdot \left| \langle Y_{lm} \,|\, \frac{\varepsilon_x + i\varepsilon_y}{\sqrt{2}} Y_{1,-1} \,|\, j, m_j \rangle \right|^2$$

Right-handed circularly polarized light preferentially excites spin-down electrons.

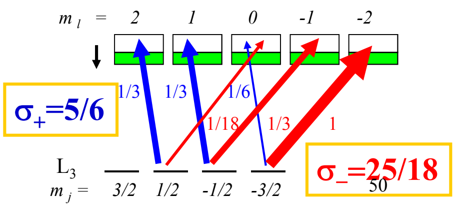

50

$$\boldsymbol{\sigma} \propto \left| \left\langle l, m_l \left| \boldsymbol{\varepsilon} \cdot \hat{\mathrm{r}} \right| j, m_j \right\rangle \right|^2$$

$$\hat{\mathrm{r}} = \left(\sin\theta\cos\phi, \sin\theta\sin\phi, \cos\theta\right)$$

$$\boldsymbol{\varepsilon} \cdot \hat{\mathrm{r}} = e_x \sin\boldsymbol{\theta}\cos\boldsymbol{\phi} + e_y \sin\boldsymbol{\theta}\sin\boldsymbol{\phi} + e_z \cos\boldsymbol{\theta}$$

$$\cos\theta = \sqrt{\tfrac{4\pi}{3}} Y_{1,0}(\theta,\phi) \quad \sin\theta \cdot e^{\pm i\phi} = \mp\sqrt{\tfrac{8\pi}{3}} Y_{1,\pm1}(\theta,\phi)$$

$$\boldsymbol{\varepsilon} \cdot \hat{\mathrm{r}} = \sqrt{\tfrac{4\pi}{3}} \left(\tfrac{-\varepsilon_x + i\varepsilon_y}{\sqrt{2}} Y_{1,1} + \tfrac{\varepsilon_x + i\varepsilon_y}{\sqrt{2}} Y_{1,-1} + \varepsilon_z Y_{1,0} \right)$$

$$\sigma_{\pm} \propto R(r)^2 \cdot \left| \left\langle Y_{lm} \left| \frac{\varepsilon_x \mp i\varepsilon_y}{\sqrt{2}} Y_{1,\pm1} \right| j, m_j \right\rangle \right|^2$$

$$\sigma_{+} \propto \left| \left\langle Y_{2,2} \left| \frac{\varepsilon_x - i\varepsilon_y}{\sqrt{2}} Y_{1,1} \right| j = \tfrac{3}{2}, m_j = \tfrac{1}{2} \right\rangle \right|^2 = \tfrac{1}{3}$$

$$\because \left\langle Y_{2,2} \left| Y_{1,1} \right| j = \tfrac{3}{2}, m_j = \tfrac{1}{2} \right\rangle = \sqrt{\tfrac{1}{3}} \left\langle Y_{2,2} \left| Y_{1,1} \right| Y_{1,1} \right\rangle = \sqrt{\tfrac{1}{3}}$$

$$\sigma_{-} \propto \left| \left\langle Y_{2,0} \left| \frac{\varepsilon_x + i\varepsilon_y}{\sqrt{2}} Y_{1,-1} \right| j = \tfrac{3}{2}, m_j = \tfrac{1}{2} \right\rangle \right|^2 = \tfrac{1}{18}$$

$$\because \left\langle Y_{2,0} \left| Y_{1,-1} \right| j = \tfrac{3}{2}, m_j = \tfrac{1}{2} \right\rangle = \sqrt{\tfrac{1}{3}} \left\langle Y_{2,0} \left| Y_{1,-1} \right| Y_{1,1} \right\rangle = \sqrt{\tfrac{1}{18}}$$

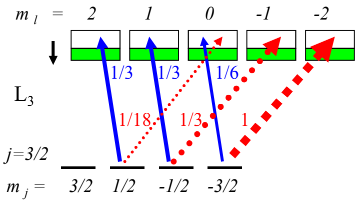

$$\left|\tfrac{3}{2},\tfrac{3}{2}\right\rangle = \left|Y_{1,1}\uparrow\right\rangle \qquad \left|\tfrac{3}{2},\tfrac{-3}{2}\right\rangle = \left|Y_{1,-1}\downarrow\right\rangle$$

$$\left|\tfrac{3}{2},\tfrac{1}{2}\right\rangle = \sqrt{\tfrac{2}{3}}\left|Y_{1,0}\uparrow\right\rangle + \sqrt{\tfrac{1}{3}}\left|Y_{1,1}\downarrow\right\rangle$$

$$\left|\tfrac{3}{2},\tfrac{-1}{2}\right\rangle = \sqrt{\tfrac{1}{3}}\left|Y_{1,-1}\uparrow\right\rangle + \sqrt{\tfrac{2}{3}}\left|Y_{1,0}\downarrow\right\rangle$$

Clesbsch-Gordan coefficients

$$Y_{lm} = \sum_{m_1 m_2} (l_1 m_1 l_2 m_2 \mid l, m) Y_{l_1 m_1} Y_{l_2 m_2}$$

$$Y_{l_1 m_1} Y_{l_2 m_2} = \sum_{l=|l_1-l_2|}^{l_1+l_2} (l_1 m_1 l_2 m_2 \mid lm) Y_{lm}$$

$$Y_{1,1}Y_{1,1} = Y_{2,2} \qquad Y_{1,-1}Y_{1,1} = \sqrt{\tfrac{1}{6}} Y_{2,0} + ...$$

51

$$\sigma \propto \left| \left\langle l, m_l \left| \boldsymbol{\varepsilon} \cdot \hat{\mathrm{r}} \right| j, m_j \right\rangle \right|^2$$

$$\boldsymbol{\varepsilon} \cdot \hat{\mathrm{r}} = \sqrt{\tfrac{4\pi}{3}} \left(\tfrac{-\varepsilon_x + i\varepsilon_y}{\sqrt{2}} Y_{1,1} + \tfrac{\varepsilon_x + i\varepsilon_y}{\sqrt{2}} Y_{1,-1} + \varepsilon_z Y_{1,0} \right)$$

$$\sigma_{\pm} \propto R(r)^2 \cdot \left| \left\langle Y_{lm} \left| \frac{\varepsilon_x \mp i\varepsilon_y}{\sqrt{2}} Y_{1,\pm1} \right| j, m_j \right\rangle \right|^2$$

$$\boldsymbol{\sigma}_{+} \propto \left| \left\langle Y_{2,1} \left| \frac{\boldsymbol{\varepsilon}_x - i\boldsymbol{\varepsilon}_y}{\sqrt{2}} Y_{1,1} \right| j = \tfrac{3}{2}, m_j = \tfrac{-1}{2} \right\rangle \right|^2 = \tfrac{1}{3}$$

$$\because \left\langle \mathbf{Y}_{2,1} \left| \mathbf{Y}_{1,1} \right| \boldsymbol{j} = \tfrac{3}{2}, \boldsymbol{m_j} = \tfrac{-1}{2} \right\rangle = \sqrt{\tfrac{2}{3}} \left\langle \mathbf{Y}_{2,1} \left| \mathbf{Y}_{1,1} \right| \mathbf{Y}_{1,0} \right\rangle = \sqrt{\tfrac{1}{3}}$$

$$Y_{1,1}Y_{1,0} = \sqrt{\tfrac{1}{2}} Y_{2,1} + ...$$

$$\sigma_{-} \propto \left| \left\langle Y_{2,-1} \left| \frac{\varepsilon_x + i\varepsilon_y}{\sqrt{2}} Y_{1,-1} \right| j = \tfrac{3}{2}, m_j = \tfrac{-1}{2} \right\rangle \right|^2 = \tfrac{1}{3}$$

$$\because \left\langle \mathbf{Y}_{2,-1} \left| \mathbf{Y}_{1,-1} \right| \boldsymbol{j} = \tfrac{3}{2}, \boldsymbol{m_j} = \tfrac{-1}{2} \right\rangle = \sqrt{\tfrac{2}{3}} \left\langle \mathbf{Y}_{2,-1} \left| \mathbf{Y}_{1,-1} \right| \mathbf{Y}_{1,0} \right\rangle = \sqrt{\tfrac{1}{3}}$$

$$Y_{1,-1}Y_{1,0} = \sqrt{\tfrac{1}{2}} Y_{2,-1} + ...$$

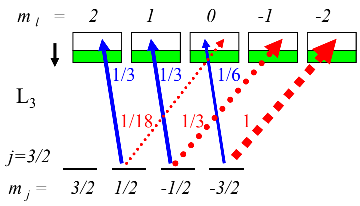

$$\left|\tfrac{3}{2},\tfrac{3}{2}\right\rangle = \left|Y_{1,1}\uparrow\right\rangle \qquad \left|\tfrac{3}{2},\tfrac{-3}{2}\right\rangle = \left|Y_{1,-1}\downarrow\right\rangle$$

$$\left|\tfrac{3}{2},\tfrac{1}{2}\right\rangle = \sqrt{\tfrac{2}{3}}\left|Y_{1,0}\uparrow\right\rangle + \sqrt{\tfrac{1}{3}}\left|Y_{1,1}\downarrow\right\rangle$$

$$\left|\tfrac{3}{2},\tfrac{-1}{2}\right\rangle = \sqrt{\tfrac{1}{3}}\left|Y_{1,-1}\uparrow\right\rangle + \sqrt{\tfrac{2}{3}}\left|Y_{1,0}\downarrow\right\rangle$$

Clesbsch-Gordan coefficients

$$Y_{lm} = \sum_{m_1 m_2} (l_1 m_1 l_2 m_2 \mid l, m) Y_{l_1 m_1} Y_{l_2 m_2}$$

$$Y_{l_1 m_1} Y_{l_2 m_2} = \sum_{l=|l_1-l_2|}^{l_1+l_2} (l_1 m_1 l_2 m_2 \mid lm) Y_{lm}$$

52

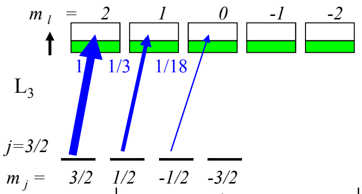

$$\sigma_+ \propto R(r)^2 \cdot \left| \left\langle Y_{lm} \left| \frac{\varepsilon_x - i\varepsilon_y}{\sqrt{2}} Y_{1,1} \right| j, m_j \right\rangle \right|^2$$

$$\sigma_+ \propto \left| \left\langle Y_{2,2} \left| \frac{\varepsilon_x - i\varepsilon_y}{\sqrt{2}} Y_{1,1} \right| j = \tfrac{3}{2}, m_j = \tfrac{3}{2} \right\rangle \right|^2 = 1$$

$$\because \left\langle Y_{2,2} \middle| Y_{1,1} \middle| j = \tfrac{3}{2}, m_j = \tfrac{3}{2} \right\rangle = \left\langle Y_{2,1} \middle| Y_{1,1} \middle| Y_{1,1} \right\rangle = 1$$

$$\sigma_+ \propto \left| \left\langle Y_{2,1} \left| \frac{\varepsilon_x - i\varepsilon_y}{\sqrt{2}} Y_{1,1} \right| j = \tfrac{3}{2}, m_j = \tfrac{1}{2} \right\rangle \right|^2 = \tfrac{1}{3}$$

$$\because \left\langle Y_{2,1} \middle| Y_{1,1} \middle| j = \tfrac{3}{2}, m_j = \tfrac{1}{2} \right\rangle = \sqrt{\tfrac{2}{3}} \left\langle Y_{2,1} \middle| Y_{1,1} \middle| Y_{1,0} \right\rangle = \sqrt{\tfrac{1}{3}}$$

$$Y_{1,1} Y_{1,0} = \sqrt{\tfrac{1}{2}} Y_{2,1} + ...$$

$$\sigma_+ \propto \left| \left\langle Y_{2,0} \left| \frac{\varepsilon_x - i\varepsilon_y}{\sqrt{2}} Y_{1,1} \right| j = \tfrac{3}{2}, m_j = \tfrac{-1}{2} \right\rangle \right|^2 = \tfrac{1}{18}$$

$$\because \left\langle Y_{2,0} \middle| Y_{1,1} \middle| j = \tfrac{3}{2}, m_j = \tfrac{1}{2} \right\rangle = \sqrt{\tfrac{1}{3}} \left\langle Y_{2,0} \middle| Y_{1,1} \middle| Y_{1,-1} \right\rangle = \sqrt{\tfrac{1}{18}}$$

$$Y_{1,1} Y_{1,-1} = \sqrt{\tfrac{1}{6}} Y_{2,0} + ...$$

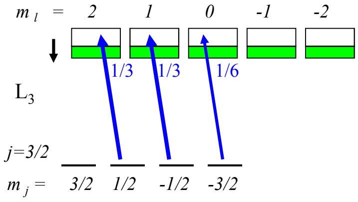

$$\left| \tfrac{3}{2}, \tfrac{3}{2} \right\rangle = \left| Y_{1,1} \uparrow \right\rangle \qquad \left| \tfrac{3}{2}, \tfrac{-3}{2} \right\rangle = \left| Y_{1,-1} \downarrow \right\rangle$$

$$\left| \tfrac{3}{2}, \tfrac{1}{2} \right\rangle = \sqrt{\tfrac{2}{3}} \left| Y_{1,0} \uparrow \right\rangle + \sqrt{\tfrac{1}{3}} \left| Y_{1,1} \downarrow \right\rangle$$

$$\left| \tfrac{3}{2}, \tfrac{-1}{2} \right\rangle = \sqrt{\tfrac{1}{3}} \left| Y_{1,-1} \uparrow \right\rangle + \sqrt{\tfrac{2}{3}} \left| Y_{1,0} \downarrow \right\rangle$$

Clesbsch-Gordan coefficients

$$Y_{lm} = \sum_{m_1 m_2} (l_1 m_1 l_2 m_2 \,|\, l, m) Y_{l_1 m_1} Y_{l_2 m_2}$$

$$Y_{l_1 m_1} Y_{l_2 m_2} = \sum_{l=|l_1 - l_2|}^{l_1 + l_2} (l_1 m_1 l_2 m_2 \,|\, lm) Y_{lm}$$

$$Y_{1,1} Y_{1,1} = Y_{2,2} \qquad Y_{1,-1} Y_{1,1} = \sqrt{\tfrac{1}{6}} Y_{2,0} + ...$$

X-ray magnetic scattering

$$\boldsymbol{H}_{\text{int}} = \overbrace{\frac{e^2}{2mc^2} \sum_j \boldsymbol{A}(\boldsymbol{r}_j)^2 + \frac{e}{mc} \sum_j \boldsymbol{A} \cdot \boldsymbol{P}_j}^{\text{kinetic energy}} \overbrace{- \frac{e\hbar}{2mc} \sum_j \boldsymbol{s}_j \cdot \nabla \times \boldsymbol{A}}^{m \cdot \mathrm{B}} \overbrace{- \frac{e^2 \hbar}{2(mc^2)^2} \sum_j \boldsymbol{s}_j \cdot \left(\frac{\partial \boldsymbol{A}}{\partial \boldsymbol{t}} \times \boldsymbol{A} \right)}^{\text{SO}}$$

Non-resonant

$$\sigma \propto \frac{2\pi}{\hbar} \left| \left\langle \boldsymbol{f} \middle| \boldsymbol{H}_{\text{int}} \middle| \boldsymbol{i} \right\rangle \right|^2$$

Blume, J. Appl. Phys. (1985)

$$= \frac{2\pi}{\hbar} \left(\frac{2\pi\hbar c^2}{V\omega} \frac{e^2}{mc^2} \right)^2 \left| \left\langle \boldsymbol{f} \middle| \sum_j e^{i\boldsymbol{q}\cdot\boldsymbol{r}_j} \middle| \boldsymbol{i} \right\rangle \varepsilon' \cdot \varepsilon - \boldsymbol{i} \frac{\hbar\omega}{mc^2} \left\langle \boldsymbol{f} \middle| \sum_j e^{i\boldsymbol{q}\cdot\boldsymbol{r}_j} \boldsymbol{s}_j \middle| \boldsymbol{i} \right\rangle \cdot \varepsilon' \times \varepsilon \right|^2$$

$$\frac{f_{\text{mag}}}{f_{\text{charge}}} \sim \frac{\hbar\omega}{mc^2} \sim 10^{-3} \qquad \frac{\sigma_{\text{mag}}}{\sigma_{\text{e}}} \sim 10^{-6}$$

for $\hbar\omega$ ~ 600 eV

Resonant

$$\sigma \propto \frac{2\pi}{\hbar} \left| \sum_n \frac{\langle \boldsymbol{f} | \boldsymbol{H}_{\text{int}} | \boldsymbol{n} \rangle \langle \boldsymbol{n} | \boldsymbol{H}_{\text{int}} | \boldsymbol{i} \rangle}{\boldsymbol{E}_i + \hbar\omega - \boldsymbol{E}_n} \right|^2 \delta(\boldsymbol{E}_i - \boldsymbol{E}_f)$$

54